Circuit Quantum Electrodynamics in Hyperbolic Space: From Photon Bound States to Frustrated Spin Models

Przemyslaw Bienias,[1,2,*] Igor Boettcher,[3,4] Ron Belyansky,[1,2] Alicia J. Kollár,[1] and Alexey V. Gorshkov[1,2]
[1]Joint Quantum Institute, University of Maryland, College Park, Maryland 20742, USA
[2]Joint Center for Quantum Information and Computer Science, NIST/University of Maryland, College Park, Maryland 20742, USA
[3]Department of Physics, University of Alberta, Edmonton, Alberta T6G 2E1, Canada
[4]Theoretical Physics Institute, University of Alberta, Edmonton, Alberta T6G 2E1, Canada

(Received 17 June 2021; accepted 15 November 2021; published 3 January 2022)

Circuit quantum electrodynamics is one of the most promising platforms for efficient quantum simulation and computation. In recent groundbreaking experiments, the immense flexibility of superconducting microwave resonators was utilized to realize hyperbolic lattices that emulate quantum physics in negatively curved space. Here we investigate experimentally feasible settings in which a few superconducting qubits are coupled to a bath of photons evolving on the hyperbolic lattice. We compare our numerical results for finite lattices with analytical results for continuous hyperbolic space on the Poincaré disk. We find good agreement between the two descriptions in the long-wavelength regime. We show that photon-qubit bound states have a curvature-limited size. We propose to use a qubit as a local probe of the hyperbolic bath, for example, by measuring the relaxation dynamics of the qubit. We find that, although the boundary effects strongly impact the photonic density of states, the spectral density is well described by the continuum theory. We show that interactions between qubits are mediated by photons propagating along geodesics. We demonstrate that the photonic bath can give rise to geometrically frustrated hyperbolic quantum spin models with finite-range or exponentially decaying interaction.

DOI: 10.1103/PhysRevLett.128.013601

One of the greatest challenges of modern physics is to formulate a consistent theory that unifies general relativity and quantum mechanics. A possible way to shed light on this problem is to study well-controlled table-top quantum simulators that mimic curved geometries [1–10]. Lattices of microwave resonators in circuit quantum electrodynamics (QED) emerged recently as a particularly promising platform [11–13]. The high control and flexibility of this system make it possible to incorporate spatial curvature in different models with strong quantum effects. Previous studies focused on understanding the properties of photons living on the hyperbolic lattice [14–24]. In this Letter, we study the impact of negative curvature on various observables of a hybrid system consisting of qubits and photons on a hyperbolic lattice.

For decades, the spectra of hyperbolic graphs have been studied by mathematicians and computer scientists due to their unusual properties [25–32]. Recently, hyperbolic graphs have also attracted the attention of the quantum error correction community [33–37]. The hyperbolic spectrum can be probed in experiments through transmission measurements [14]. Here, we propose to use qubits to probe the local properties of hyperbolic graphs.

Classical spin models on hyperbolic lattices were studied in Refs. [38–44]. However, the quantum spin model problem [45–48] is more challenging due to the interplay of quantum mechanics with noncommutative geometry and strong geometric frustration. In the spirit of quantum simulation, we propose to use a hybrid photon-qubit system to engineer (i) finite-range localized photon-mediated interactions between spins, and (ii) exponentially decaying photon-mediated interactions. Finally, our work is related to recent studies of emitters interacting with structured quantum baths [49–53].

System.—We study a circuit QED system with photons and qubits on a hyperbolic lattice $\mathcal{G}$. The photons are modeled by a tight-binding Hamiltonian, and the qubits, at positions i, are approximated by two-level systems with spin-1/2 operators $\sigma_i^+\sigma_i^- = |\uparrow\rangle\langle\uparrow|_i$. The full Hamiltonian in the rotating-wave approximation and rotating frame reads as

$$\hat{H} = \Delta\sum_{i\in\mathcal{S}}|\uparrow\rangle\langle\uparrow|_i + g\sum_{j\in\mathcal{S}}(\sigma_j^+ a_j + \text{H.c.}) + \hat{H}_{\text{ph}}, \quad (1)$$

$$\hat{H}_{\text{ph}} = -t\sum_{\langle ij\rangle\in\mathcal{G}} a_i^\dagger a_j, \quad (2)$$

with $a_i^\dagger$ the photon creation operator, g the coupling between photons and qubits, and Δ the difference between the qubit frequency and the frequency of a photon on a single site. The set $\mathcal{S}$ comprises the qubit sites and $\mathcal{G}$ the

hyperbolic lattice. For concreteness, in the following we set the hopping $t = 1$.

The spectrum of $\hat{H}_{\rm ph}$ is bounded from below and above [54,55] [see Fig. 1(a)], and hence the spectrum of $\hat{H}$ consists of scattering eigenstates together with localized photon-qubit bound states [49,56–60]. For a single qubit at position i, the single-excitation eigenstate energies ω are given by the solutions of

$$\omega = \Delta + g^2 G_{ii}(\omega), \tag{3}$$

where $G_{ij}(\omega) = (\omega - \hat{H}_{\rm ph})^{-1}_{ij}$ is the photonic Green function. We denote the lowest eigenvalue of $\hat{H}_{\rm ph}$ or lower band edge (LEBE) by $E_0 < 0$. For arbitrary Δ, Eq. (3) always permits two solutions outside the photonic band (corresponding to the bound states), and we focus in the following on the lower bound state with $\omega = E_B < \Delta$. For weak coupling ($g \ll |E_0 - \Delta|$), we have $E_B \approx \Delta + g^2 G_{ii}(\Delta)$, and the bound-state wave function consists mostly of the spin component such that

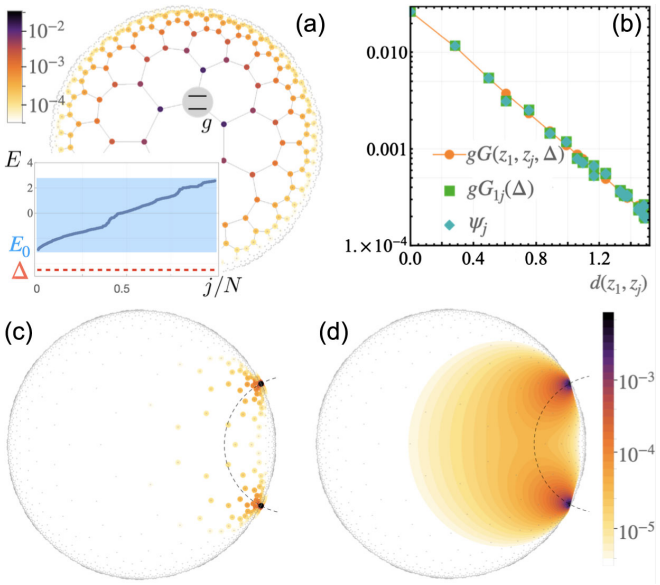

FIG. 1. (a) Single-excitation single-qubit bound state. Color indicates the amplitude of the wave function. Gray lines denote the connectivity of photonics sites. One site is coupled via g to a qubit (gray circle). Inset: the photonic spectrum as a function of the eigenstate index j. All results are for $g = 0.05$ and $\Delta = -3.2$ below the band edge at $E_0 \approx -2.9$. (b) Comparison of photonic amplitudes of the lowest eigenstate as a function of the distance $d(z_1, z_j)$ from the qubit at z_1—exact ψ_j (diamonds), perturbative expressions from Eq. (4) based on discrete (squares) and continuous (dots) Green function. (c) and (d) The density of the photonic amplitude of a two-spin single-excitation bound state illustrating the photon-mediated interactions between spins on the graph (c) and in the continuum (d). We see that photons follow the shortest path between two spins [positioned at two black dots in (c)]—the geodesic shown as a (dashed) semicircle on the Poincaré disk.

$$|\psi_B\rangle \approx |\uparrow, 0\rangle + g \sum_{j \in \mathcal{G}} G_{ij}(\Delta) a_j^\dagger |\downarrow, 0\rangle. \tag{4}$$

When the experimentally relevant energies are close to the LEBE, $\omega - E_0 \lesssim t$, we can capture the photonic part by a continuum model [16] on the Poincaré disk with metric $ds^2 = (2\kappa)^2 (dx^2 + dy^2)/(1 - r^2)^2$ and curvature radius $\kappa = 1/2$ [61]. The finite hyperbolic lattice is mapped to a hyperbolic disk of radius $L < 1$, where $L = \sqrt{N/(N + N_0)}$ for N sites with N_0 a constant [16], so that $L \to 1$ for large lattices. For concreteness, we consider the $\{7, 3\}$ lattice based on regular heptagons with coordination number 3, with $N_0 = 28$, and lattice constant $h = 0.276$. However, our results apply (i) to other hyperbolic $\{p, q\}$ lattices by substituting the corresponding value of h, and (ii) to line graphs of $\{p, q\}$ lattices [54] in the long-wavelength regime. We denote the hyperbolic distance by $d(z, z') = \kappa \operatorname{arcosh}(1 + \{[2|z - z'|^2]/[(1 - |z|^2)(1 - |z'|^2)]\})$. The number $d(z_i, z_j)$, intuitively, quantifies the number of hops needed to get from z_i to z_j on the graph.

The photon spectrum is continuous on the Poincareé disk and given by $E_{\mathbf{k}} = E_0 + (1/M)|\mathbf{k}|^2$, with momentum $\mathbf{k}$, effective photon mass $M = (4/3h^2)$ [16]. The bound-state condition [Eq. (3)] becomes $E_B = \Delta + g^2 G_\Lambda(z_i, z_i, E_B)$, with $G_\Lambda(z, z', \omega)$ the continuum approximation of the photon Green function. The subscript Λ indicates the need to introduce a large-momentum cutoff $\Lambda \propto h^{-1}$, because the continuum Green function is not well defined for $z = z'$ [16]. This is analogous to the well-known regularization of bound states for parabolic bands in two Euclidean dimensions [62,63]. The value of Λ can be fixed through a renormalization condition, yielding $\Lambda \simeq 3h^{-1}$ [64]. The bound-state wave function for a qubit at z_i, for arbitrary $L < 1$ and energies close to the LEBE, is

$$|\psi_B\rangle \propto \left(\sigma_i^+ - \int \frac{d^2 z}{(1 - |z|^2)^2} u(z) a^\dagger(z)\right) |\downarrow, 0\rangle, \tag{5}$$

with $u(z) = M\tilde{g} G_\Lambda(z_i, z, E_B)$ and $\tilde{g} = \sqrt{\pi/28} g$. In Fig. 1(b), we show the photonic amplitude $|u(z)|$ of the bound-state wave function using both the continuum expression for $G_\Lambda(z_i, z_j, E_B)$ from Ref. [16] and lattice Green function $G_{ij}(E_B)$, which both agree well with the exact result.

Setting $L = 1$ in the continuum model, i.e., considering an infinite system, often leads to simple analytical formulas, but assumes the absence of a system boundary. Since boundary effects are not subleading in hyperbolic space, results obtained for $L = 1$ can differ *qualitatively* from those for any $L < 1$, which is the case for our system. We are primarily interested in contributions of weakly coupled spins located in the bulk, sufficiently far away from the boundary. We find that some observables are well captured by the $L = 1$ limit, whereas others need to be computed for $L < 1$. The continuum Green function for $L = 1$ reads

$$G_\Lambda(z_i, z_i, E_B) = \frac{\pi}{28}\int_{k\le\Lambda}\frac{d^2k}{(2\pi)^2}\frac{\tanh(\pi k/2)}{E_B - E_0 - \frac{1}{M}k}, \quad (6)$$

where $k = |\mathbf{k}|$. The tanh term in the numerator [65] is due to the negative curvature of space. In practice, $|E_B - E_0| \gg M^{-1}$ because of the large value of the mass, and we can neglect the tanh factor to approximate $G_\Lambda(z_i, z_i, E_B) \approx (M/112)\ln(|E_B - E_0|M/\Lambda^2)$.

Curvature-limited correlations.—The continuum approximation enables us to analytically quantify the size of the single-particle bound state. For this purpose, we expand [64] the Green function for large hyperbolic distance $d(z, z') \gg h$, leading to

$$G_\Lambda(z, z', \omega) \approx G_\Lambda^{(0)}(\omega)\exp\left(-\frac{d(z, z')}{2\xi(\omega)}\right), \quad (7)$$

which confirms the exponential decay shown in Fig. 1(b). The correlation length ξ depends on the system parameters through the frequency ω, and in the following we neglect a weak residual dependence on z and z' from boundary effects. In the continuum approximation and in the limit $L \to 1$, the lower edge of the photonic band is located at $E_0 = -3 + (1/M)$ [16]. As ω approaches E_0 from below, for qubits coupled to a Euclidean lattice, the correlation length diverges as $\xi \propto (E_0 - \omega)^{-1/2}$ [50,56]. In stark contrast, on the hyperbolic lattice, correlations are cut off by the curvature radius, and $\xi \le \kappa$ remains finite. In particular, for $L = 1$ and $\omega < E_0$, we find [64] that

$$\xi \approx \frac{\kappa}{1 + \sqrt{M(E_0 - \omega)}}. \quad (8)$$

Spin relaxation and photonic density of states (DOS).—We propose a local probe—an excited qubit with frequency within the band—to measure properties of hyperbolic graphs. For very weak coupling g, one can couple to only a few eigenstates and extract the spectral properties from the time dependence of the excited state population. On the other hand, by using larger g, such that a qubit couples to many states, the dynamics of the initially excited spin corresponds to the exponential decay governed by the graph spectrum. We concentrate on the latter in the following.

The spontaneous emission from the qubit can be described by a Markovian Lindblad master equation with the decay rate $\Gamma = j(\Delta)$, where $j(\omega) = 2\pi\sum_{\mathbf{k}}|g_{\mathbf{k}}|^2\delta(\omega - \omega_{\mathbf{k}})$ is the spectral function. In the low-energy continuum approximation we have $g_{\mathbf{k}} = g\sqrt{(\pi/28)}|\psi_{\mathbf{k}}(z_i)|$ with $\psi_{\mathbf{k}}(z)$ the eigenfunctions of the hyperbolic Laplacian [64] and $\omega_{\mathbf{k}} = E_0 + (1/M)|\mathbf{k}|^2$. Furthermore, for $L = 1$, we have

$$j_{L=1}(\omega) = \frac{\pi M}{56}g^2\tanh\left(\frac{\pi\sqrt{(\omega - E_0)M}}{2}\right). \quad (9)$$

We see that, due to the tanh factor, $j(\omega)$ is qualitatively different in curved space than in 2D Euclidean space where, for quadratic dispersion, $j(\omega)$ lacks this factor and is thus constant. However, the range of energies for which curved and flat space differ is restricted to a narrow energy range $\lesssim\delta E_{L=1} = 1/M \ll 1$ close to the LEBE. Note that, for $L = 1$ and within the continuum approximation, $j(\omega)$ is directly proportional to the DOS ρ, $\rho_{L=1} = N\eta\tanh[(\pi/2)\sqrt{(\omega - E_0)M}]$ with $\eta = (M/112)$, as the energy dependence from $g_{\mathbf{k}}$ drops out in the angular average [64], as is often the case in the Euclidean geometry [52].

Close to the LEBE, the photonic spectrum can be computed from the hyperbolic Laplacian Δ_g for any $L < 1$ using Dirichlet boundary conditions. The DOS of eigenvalues ε of the Laplacian follows Weyl's law $\rho_W(\varepsilon) \sim (\text{area}/4\pi) - [\text{circ}/(8\pi\sqrt{\varepsilon})] + \mathcal{O}(\varepsilon^{-1})$ [66–69], with area $= \pi L^2/(1 - L^2)$ and circ $= 2\pi L/(1 - L^2)$ the area and circumference of the finite hyberbolic disk, respectively. Using $\varepsilon = M(\omega - E_0)$, we arrive at

$$\rho_W(\omega) \approx \frac{L^2/h^2}{3(1 - L^2)} - \frac{L/h}{2\sqrt{3}(1 - L^2)}\frac{1}{\sqrt{\omega - E_0}}. \quad (10)$$

Note that the leading, constant term is characteristic for parabolic bands in two dimensions, but the subleading correction is important even in the large-system limit—which is in dramatic contrast to flat space. Importantly, setting $L = 1$ in ρ_W does not reproduce $\rho_{L=1}$.

In Fig. 2(a), we plot the exact normalized cumulative DOS, $P(\omega) = (1/N)\int_{E_0}^{\omega} d\nu\rho(\nu)$, from which we see that P shows Weyl scaling and does not change with system size. We confirm that the second term in Weyl's law [Eq. (10)] is non-negligible in a wide range of energies, δE_W, which is much greater than $\delta E_{L=1}$. The neglect of boundary effects

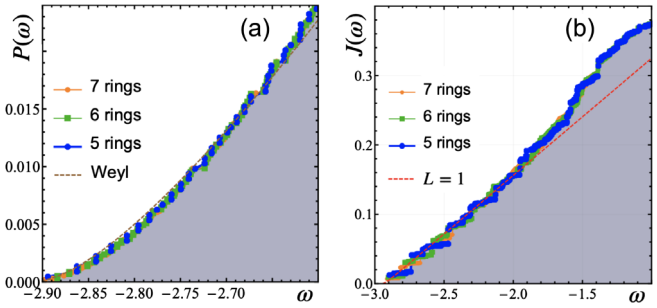

FIG. 2. Comparison of spectral properties from analytic limits to numerics of different-sized graphs in the long-wavelength limit near the LEBE. Graphs are characterized by the number ℓ of concentric rings of heptagons, where $\ell = 1$ corresponds to a single heptagon. (a) The cumulative DOS $P(\omega)$ has data points nearly overlapping for different ℓ. (b) The cumulative $J(\omega)$ is less smooth, but asymptotically ($\ell \to \infty$) approaches $J_{L=1}(\omega)$: The root-mean-square error with respect to $J_{L=1}$ for $\omega < -2$ is 0.0066, 0.0052, and 0.0044 for $\ell = 5$, 6, and 7, respectively.

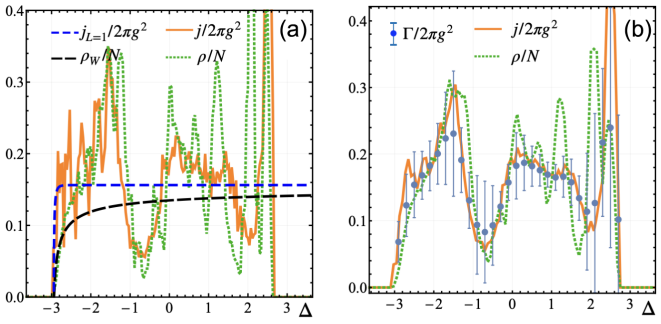

FIG. 3. (a) Comparison of analytical expressions and numerical results (with the bin size $\Delta\omega = 0.15$) for j and ρ. (b) Comparison of the numerical (with $\Delta\omega = 0.3$) j and ρ with the fitted Γ within time $\in [0, 15]$ (error bars correspond to the standard deviation) for $g = 0.3$, $\ell = 7$.

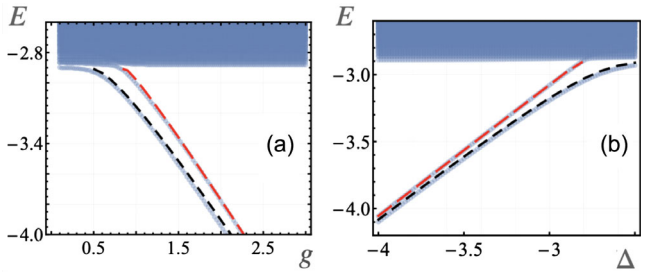

FIG. 4. Energy spectrum (a) as a function of g for $\Delta = -2.5$ and next-nearest neighbors separated by $z = 0.5$, and (b) as a function of Δ for $g = 0.5$ and nearest neighbors separated by $z = h = 0.276$. All lattice results are for $\ell = 6$, which we compare with symmetric (lower black dashed curve) and antisymmetric (upper red dashed) 2-qubit bound states.

in $\rho_{L=1}$ does not reproduce the lattice DOS. Note that the leading term in ρ_W is the same as the large-ω value of $\rho_{L=1}(\omega)$, which is equal to $N\eta$.

Figure 2(b) shows the cumulative spectral function $J(\omega) = \int_{E_0}^{\omega} d\nu j(\nu)/g^2$. Close to the band edge, we observe that $J(\omega)$ with increasing ℓ is well approximated by a constant $j(\omega)$. Hence, $J(\omega)$ qualitatively agrees [70] with $j_{L=1}(\omega)$, because both lead to a nearly constant value of $j(\omega)$. We conclude that, since $j(\omega)$ is a *local* quantity, it is only weakly influenced by the boundary physics of hyperbolic lattices and can be described by the continuum $L = 1$ theory, which is an important and useful result for future experimental and theoretical studies.

The presence of the lattice leads to a significant difference between ρ and j for large Δ away from the LEBE [see Fig. 3(a)], whereas they are directly proportional in the low-energy continuum approximation for $L = 1$. We numerically extract the decay rate Γ on the lattice from the dynamics of an initially excited spin with no photons, however, with significant error bars for some detunings Δ corresponding to the nonexponential decay. Due to the limited lattice sizes accessible in numerics, we analyzed $g = 0.3$ to ensure that the qubit is coupled to many photonic modes. We find that $\Gamma \propto j(\omega)$ rather than $\propto \rho$ [see Fig. 3(b)]. The deviation between Γ and j is caused by (i) the finite number of states we couple to, (ii) edge effects such as reflection from the boundary, (iii) fast variation of the photonic density of states with energy, and (iv) effects beyond Fermi's golden rule due to g being comparable to the hopping strength $t = 1$. These effects can also contribute to the error bars in Fig. 3(b). We note that for larger systems, one could either suppress or better establish nonexponential decay.

Single-excitation bound state for 2 qubits.—We now consider 2 qubits located at positions z_1 and z_j, each with frequency Δ. In this case, the situation is slightly different than for 1 qubit. There is always one symmetric bound state below the LEBE for all Δ, but for certain unfavorable values of Δ, distance between qubits, or coupling strength, the second antisymmetric bound state melts into the continuum of states. This is analogous to antisymmetric bound states in 1D [49]. The energies of two single-excitation bound states ($E_B^{\pm}$) are given by the solutions of

$$E_B^{\pm} - \Delta - \Sigma_{11}(E_B^{\pm}) \mp \Sigma_{1j}(E_B^{\pm}) = 0, \tag{11}$$

with $\Sigma_{ij}(\omega) = g^2 G_{ij}(\omega)$. We find good agreement between the solution using the continuum Green function $G_\Lambda(z_i, z_j, \omega)$ and the results using the lattice Green function $G_{ij}(\omega)$ (see Fig. 4).

The bound-state wave functions in the continuum are

$$|\psi_B^{\pm}\rangle = c_{\pm}\Big[(\sigma_1^+ \pm \sigma_j^+) - \frac{4\tilde{g}}{3th^2}\int_z [G_\Lambda(z, z_1; E_B^{\pm}) \pm G_\Lambda(z, z_j; E_B^{\pm})]a^\dagger(z)\Big]|{\downarrow\downarrow}0\rangle. \tag{12}$$

In Figs. 1(c) and 1(d), we plot the photonic density for the lowest (i.e., symmetric) bound state $|\psi_B^+\rangle$ as a function of position z. On a lattice, z takes only discrete values z_i, and $n_{\rm ph}(z_i)$ is given by $g^2 \sum_{w,w' \in \{1,j\}} G_{wi}(E_B) G_{w'i}(E_B)$. We see that the photons mediating the interactions follow a geodesic—the shortest path between the two spins.

Effective spin models.—The coupling of spins to the hyperbolic photonic bath leads to an effective spin-spin interaction that changes as the spin frequency is tuned. For spin frequencies satisfying $E_0 - \Delta \gg g$, we integrate out the hyperbolic photons and arrive at the effective spin-spin Hamiltonian

$$\hat{V} = g^2 \sum_{ij} G_{ij}(\Delta)\sigma_i^- \sigma_j^+ \tag{13}$$

describing flip-flop interactions. Here terms with $i = j$ introduce an on site energy shift for the qubits. For $i \neq j$, we can use the continuum approximation for the Green function $G_{ij}(\omega)$. Equation (7) reveals that the interaction

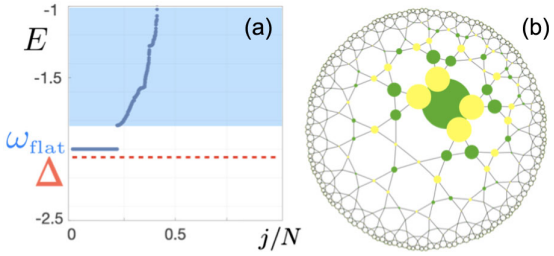

FIG. 5. Spin model in the vicinity of the flatband for the heptagonal kagomelike line graph with $t = -1$ [14]. (a) The photonic spectrum as a function of the eigenstate index j. (b) We plot the interaction strength as a function of qubit position, assuming the position of the second qubit to be where the largest dot is. The dot color denotes the sign of the interactions [green (yellow) is $+(-)$], whereas its diameter is directly proportional to the interaction strength.

decays exponentially with a correlation length $\xi \leq \kappa = 1/2$ that depends on Δ.

For simplicity of presentation, we focused on hyperbolic $\{p, q\}$ graphs. Conveniently, their long-wavelength physics is the same as that of their line graphs [71], which naturally appear in cQED experiments [14]. Line graphs, additionally, feature a flatband of localized states at energy ω_{flat}, which is near the LEBE for $t < 0$ [14]. In particular, for lattices based on polygons with an odd number of vertices, these flatbands are gapped [see Fig. 5(a)]. Due to the gap, we can choose the qubits to be coupled effectively only to the flatband. Because flatband eigenstates have support only on two neighboring polygons [14], the photon-mediated interactions between the spins are strictly finite range. The spin Hamiltonian, in terms of the wave functions ϕ_k describing the localized states in the flatband, reads as

$$\hat{V} = \frac{g^2}{\Delta - \omega_{\text{flat}}} \sum_{k,ij} \phi_k^*(z_j)\phi_k(z_i)\sigma_i^- \sigma_j^+. \tag{14}$$

Figure 5 illustrates that the interactions are of finite range, with the sign of the interactions oscillating rapidly with distance (see Supplemental Material [64]). Together with possible geometric frustration, this leads to a highly frustrated spin model, which may lead to exotic spin-liquid phases.

Outlook.—Though we assumed two-level qubits, the multilevel structure of different superconducting qubits is worth exploring, for example, of transmon [72] or fluxonium [73]. In a regime in which the anharmonicity of the transmon is not large enough to neglect higher excited levels, we envision a generalized hyperbolic Bose-Hubbard model with long-range hopping. On the other hand, fluxonium qubits offer larger anharmonicities as well as enable Raman and microwave-activated (possibly time-dependent) control [74,75]. Using our formalism, it is exciting to study the impact of spatial curvature on the creation and detection of entanglement, fractional quantum Hall phases [17,76], giant atoms [77], frustrated and/or disordered spin and bosonic models [78,79], and BCS theory involving flatbands [80]. Finally, we envision the possibility of engineering a quantum simulator of the AdS-CFT correspondence [81,82].

P. B., I. B, R. B., and A. V. G. acknowledge support by National Science Foundation Quantum Leap Challenge Institute (Grant No. OMA-2120757), Air Force Office of Scientific Research, Air Force Office of Scientific Research Multidisciplinary University Research Initiative, National Science Foundation Physics Frontier Center at the Joint Quantum Institute, Army Research Office Multidisciplinary University Research Initiative, Department of Energy Advanced Scientific Computing Research Quantum Testbed Pathfinder program (Award No. DE-SC0019040), U.S. Department of Energy Award No. DE-SC0019449, Department of Energy Advanced Scientific Computing Research Accelerated Research in Quantum Computing program (Award No. DE-SC0020312), and National Science Foundation Practical Fully-Connected Quantum Computer program. I. B. acknowledges support from the University of Alberta startup fund UOFAB Startup Boettcher. R. B. also acknowledges support of Natural Sciences and Engineering Research Council of Canada and Fonds de recherche du Québec – Nature et technologies of Canada. A. J. K. acknowledges support from Airforce Office of Scientific Research Grant No. FA95502110129, National Science Foundation Grant No. PHY2047732, and National Science Foundation Quantum Leap Challenge Institute for Robust Quantum Simulation (Grant No. OMA2120757).

*przemyslaw.bienias@gmail.com

[1] U. Leonhardt and P. Piwnicki, Relativistic Effects of Light in Moving Media with Extremely Low Group Velocity, Phys. Rev. Lett. **84**, 822 (2000).
[2] D. A. Genov, S. Zhang, and X. Zhang, Mimicking celestial mechanics in metamaterials, Nat. Phys. **5**, 687 (2009).
[3] I. I. Smolyaninov and E. E. Narimanov, Metric Signature Transitions in Optical Metamaterials, Phys. Rev. Lett. **105**, 067402 (2010).
[4] R. Bekenstein, R. Schley, M. Mutzafi, C. Rotschild, and M. Segev, Optical simulations of gravitational effects in the Newton-Schrödinger system, Nat. Phys. **11**, 872 (2015).
[5] L. J. Garay, J. R. Anglin, J. I. Cirac, and P. Zoller, Sonic Analog of Gravitational Black Holes in Bose-Einstein Condensates, Phys. Rev. Lett. **85**, 4643 (2000).
[6] P. O. Fedichev and U. R. Fischer, Gibbons-Hawking Effect in the Sonic de Sitter Space-Time of an Expanding Bose-Einstein-Condensed Gas, Phys. Rev. Lett. **91**, 240407 (2003).

[7] D. E. Chang, A. S. Sørensen, E. A. Demler, and M. D. Lukin, A single-photon transistor using nanoscale surface plasmons, Nat. Phys. **3**, 807 (2007).

[8] C. Sheng, H. Liu, Y. Wang, S. N. Zhu, and D. A. Genov, Trapping light by mimicking gravitational lensing, Nat. Photonics **7**, 902 (2013).

[9] O. Lahav, A. Itah, A. Blumkin, C. Gordon, S. Rinott, A. Zayats, and J. Steinhauer, Realization of a Sonic Black Hole Analog in a Bose-Einstein Condensate, Phys. Rev. Lett. **105**, 240401 (2010).

[10] J. Hu, L. Feng, Z. Zhang, and C. Chin, Quantum simulation of Unruh radiation, Nat. Phys. **15**, 785 (2019).

[11] A. A. Houck, H. E. Türeci, and J. Koch, On-chip quantum simulation with superconducting circuits, Nat. Phys. **8**, 292 (2012).

[12] M. Fitzpatrick, N. M. Sundaresan, A. C. Y. Li, J. Koch, and A. A. Houck, Observation of a Dissipative Phase Transition in a One-Dimensional Circuit QED Lattice, Phys. Rev. X **7**, 011016 (2017).

[13] B. M. Anderson, R. Ma, C. Owens, D. I. Schuster, and J. Simon, Engineering Topological Many-Body Materials in Microwave Cavity Arrays, Phys. Rev. X **6**, 041043 (2016).

[14] A. J. Kollár, M. Fitzpatrick, and A. A. Houck, Hyperbolic lattices in circuit quantum electrodynamics, Nature (London) **571**, 45 (2019).

[15] L. Boyle, M. Dickens, and F. Flicker, Conformal Quasicrystals and Holography, Phys. Rev. X **10**, 011009 (2020).

[16] I. Boettcher, P. Bienias, R. Belyansky, A. J. Kollár, and A. V. Gorshkov, Quantum simulation of hyperbolic space with circuit quantum electrodynamics: From graphs to geometry, Phys. Rev. A **102**, 032208 (2020).

[17] S. Yu, X. Piao, and N. Park, Topological Hyperbolic Lattices, Phys. Rev. Lett. **125**, 053901 (2020).

[18] R. C. Brower, C. V. Cogburn, A. L. Fitzpatrick, D. Howarth, and C.-I. Tan, Lattice setup for quantum field theory in AdS_2, Phys. Rev. D **103**, 094507 (2021).

[19] M. Asaduzzaman, S. Catterall, J. Hubisz, R. Nelson, and J. Unmuth-Yockey, Holography on tessellations of hyperbolic space, Phys. Rev. D **102**, 034511 (2020).

[20] J. Maciejko and S. Rayan, Hyperbolic band theory, Sci. Adv. **7**, eabe9170 (2021).

[21] R. Zhang, C. Lv, Y. Yan, and Q. Zhou, Efimov-like states and quantum funneling effects on synthetic hyperbolic surfaces, Sci. Bull. **66**, 1967 (2021).

[22] C. Sheng, C. Huang, R. Yang, Y. Gong, S. Zhu, and H. Liu, Simulating the escape of entangled photons from the event horizon of black holes in nonuniform optical lattices, Phys. Rev. A **103**, 033703 (2021).

[23] X. Zhu, J. Guo, N. P. Breuckmann, H. Guo, and S. Feng, Quantum phase transitions of interacting bosons on hyperbolic lattices, arXiv:2103.15274.

[24] I. Boettcher, A. V. Gorshkov, A. J. Kollár, J. Maciejko, S. Rayan, and R. Thomale, Crystallography of hyperbolic lattices, arXiv:2105.01087.

[25] W. Woess, Context-free languages and random walks on groups, Discrete Math. **67**, 81 (1987).

[26] T. Sunada, Group C^*-algebras and the spectrum of a periodic Schrödinger operator on a manifold, Can. J. Math. **44**, 180 (1992).

[27] W. J. Floyd and S. P. Plotnick, Growth functions on Fuchsian groups and the Euler characteristic, Inventiones Mathematicae **88**, 1 (1987).

[28] L. Bartholdi and T. G. Ceccherini-Silberstein, Growth series and random walks on some hyperbolic graphs, Monatshefte fur Mathematik **136**, 181 (2002).

[29] R. S. Strichartz, Harmonic analysis as spectral theory of Laplacians, J. Funct. Anal. **87**, 51 (1989).

[30] S. Agmon, Spectral theory of Schrödinger operators on euclidean and on non-euclidean spaces, Commun. Pure Appl. Math. **39**, S3 (1986).

[31] D. Krioukov, F. Papadopoulos, M. Kitsak, A. Vahdat, and M. Boguñá, Hyperbolic geometry of complex networks, Phys. Rev. E **82**, 036106 (2010).

[32] M. Boguñá, F. Papadopoulos, and D. Krioukov, Sustaining the internet with hyperbolic mapping, Nat. Commun. **1**, 62 (2010).

[33] F. Pastawski, B. Yoshida, D. Harlow, and J. Preskill, Holographic quantum error-correcting codes: Toy models for the bulk/boundary correspondence, J. High Energy Phys. 06 (2015) 001.

[34] N. P. Breuckmann and B. M. Terhal, Constructions and noise threshold of hyperbolic surface codes, IEEE Trans. Inf. Theory **62**, 3731 (2016).

[35] N. P. Breuckmann, C. Vuillot, E. Campbell, A. Krishna, and B. M. Terhal, Hyperbolic and semi-hyperbolic surface codes for quantum storage, Quantum Sci. Technol. **2**, 035007 (2017).

[36] A. Lavasani, G. Zhu, and M. Barkeshli, Universal logical gates with constant overhead: Instantaneous Dehn twists for hyperbolic quantum codes, Quantum **3**, 180 (2019).

[37] A. Jahn and J. Eisert, Holographic tensor network models and quantum error correction: A topical review, Quantum Sci. Tech. **6**, 033002 (2021).

[38] R. Rietman, B. Nienhuis, and J. Oitmaa, The Ising model on hyperlattices, J. Phys. A **25**, 6577 (1992).

[39] H. Shima and Y. Sakaniwa, Geometric effects on critical behaviours of the Ising model, J. Phys. A **39**, 4921 (2006).

[40] S. K. Baek, S. D. Yi, and B. J. Kim, Diffusion on a heptagonal lattice, Phys. Rev. E **77**, 022104 (2008).

[41] R. Krcmar, A. Gendiar, K. Ueda, and T. Nishino, Ising model on a hyperbolic lattice studied by the corner transfer matrix renormalization group method, J. Phys. A **41**, 125001 (2008).

[42] S. K. Baek, P. Minnhagen, and B. J. Kim, Percolation on hyperbolic lattices, Phys. Rev. E **79**, 011124 (2009).

[43] H. Gu and R. M. Ziff, Crossing on hyperbolic lattices, Phys. Rev. E **85**, 051141 (2012).

[44] M. Serina, J. Genzor, Y. Lee, and A. Gendiar, Free-energy analysis of spin models on hyperbolic lattice geometries, Phys. Rev. E **93**, 042123 (2016).

[45] H. J. Changlani, S. Ghosh, S. Pujari, and C. L. Henley, Emergent Spin Excitations in a Bethe Lattice at Percolation, Phys. Rev. Lett. **111**, 157201 (2013).

[46] H. J. Changlani, S. Ghosh, C. L. Henley, and A. M. Läuchli, Heisenberg antiferromagnet on Cayley trees: Low-energy spectrum and even/odd site imbalance, Phys. Rev. B **87**, 085107 (2013).

[47] M. Daniska and A. Gendiar, Analysis of quantum spin models on hyperbolic lattices and Bethe lattice, J. Phys. A **49**, 145003 (2016).

[48] A. Chapman and S. T. Flammia, Characterization of solvable spin models via graph invariants, Quantum **4**, 278 (2020).
[49] G. Calajó, F. Ciccarello, D. Chang, and P. Rabl, Atom-field dressed states in slow-light waveguide QED, Phys. Rev. A **93**, 033833 (2016).
[50] T. Shi, Y. H. Wu, A. Gonzalez-Tudela, and J. I. Cirac, Bound States in Boson Impurity Models, Phys. Rev. X **6**, 021027 (2016).
[51] T. Shi, Y. H. Wu, A. González-Tudela, and J. I. Cirac, Effective many-body Hamiltonians of qubit-photon bound states, New J. Phys. **20**, 105005 (2018).
[52] A. González-Tudela and J. I. Cirac, Quantum Emitters in Two-Dimensional Structured Reservoirs in the Nonperturbative Regime, Phys. Rev. Lett. **119**, 143602 (2017).
[53] A. González-Tudela and J. I. Cirac, Markovian and non-Markovian dynamics of quantum emitters coupled to two-dimensional structured reservoirs, Phys. Rev. A **96**, 043811 (2017).
[54] A. J. Kollár, M. Fitzpatrick, P. Sarnak, and A. A. Houck, Line-graph lattices: Euclidean and non-euclidean flat bands, and implementations in circuit quantum electrodynamics, Commun. Math. Phys. **376**, 1909 (2020).
[55] A. J. Kollár and P. Sarnak, Gap sets for the spectra of cubic graphs, arXiv:2005.05379.
[56] N. M. Sundaresan, R. Lundgren, G. Zhu, A. V. Gorshkov, and A. A. Houck, Interacting Qubit-Photon Bound States with Superconducting Circuits, Phys. Rev. X **9**, 011021 (2019).
[57] E. Munro, A. Asenjo-Garcia, Y. Lin, L. C. Kwek, C. A. Regal, and D. E. Chang, Population mixing due to dipole-dipole interactions in a 1D array of multilevel atoms, Phys. Rev. A **98**, 033815 (2018).
[58] Y. Liu and A. A. Houck, Quantum electrodynamics near a photonic bandgap, Nat. Phys. **13**, 48 (2017).
[59] C. L. Hung, A. González-Tudela, J. I. Cirac, and H. J. Kimble, Quantum spin dynamics with pairwise-tunable, long-range interactions, Proc. Natl. Acad. Sci. U.S.A. **113**, E4946 (2016).
[60] J. S. Douglas, T. Caneva, and D. E. Chang, Photon Molecules in Atomic Gases Trapped Near Photonic Crystal Waveguides, Phys. Rev. X **6**, 031017 (2016).
[61] J. W. Cannon, W. J. Floyd, R. Kenyon, and W. R. Parry, Hyperbolic geometry, in *Flavors of Geometry* edited by S. Levy (Cambridge University Press, Cambridge, England, 1997), Vol. 31.
[62] M. Randeria, J.-M. Duan, and L.-Y. Shieh, Bound States, Cooper Pairing, and Bose Condensation in Two Dimensions, Phys. Rev. Lett. **62**, 981 (1989).
[63] S. Schmitt-Rink, C. M. Varma, and A. E. Ruckenstein, Pairing in Two Dimensions, Phys. Rev. Lett. **63**, 445 (1989).
[64] See Supplemental Material at http://link.aps.org/supplemental/10.1103/PhysRevLett.128.013601 for the discussion of the ultraviolet cutoff and the detailed derivations of: The qubit-photon Hamiltonian within the low-energy continuum approximation, Eq. (8), the bound-state equations for a single qubit and for 2 qubits, and the spontaneous emission rate of an excited qubit within the continuum approximation.
[65] S. Helgason, Non-euclidean analysis, in *Non-Euclidean Geometries*, edited by A. Prekopa and E. Molnar (Springer, New York, 2006).
[66] W. Krauth, *Statistical Mechanics* (Butterworth-Heinemann, London, 2006), Chap. 10, p. 354.
[67] V. Ya Ivrii, Second term of the spectral asymptotic expansion of the Laplace—Beltrami operator on manifolds with boundary, Funct. Anal. Appl. **14**, 98 (1980).
[68] B. Osgood, R. Phillips, and P. Sarnak, Extremals of determinants of Laplacians, J. Funct. Anal. **80**, 148 (1988).
[69] A. Aydin, T. Oikonomou, G. B. Bagci, and A. Sisman, Discrete and Weyl density of states for photons and phonons, Phys. Scr. **94**, 105001 (2019).
[70] Except in a frequency window of size $\delta E_{L=1} \ll 1$ near the $>$ band edge, which we cannot resolve numerically with finite lattices, and $>$ thus cannot resolve the tanh-factor in Eq. (9).
[71] For line graphs, for $t < 0$, the long-wavelength part of the spectrum corresponds to high energies.
[72] J. Koch, T. M. Yu, J. Gambetta, A. A. Houck, D. I. Schuster, J. Majer, A. Blais, M. H. Devoret, S. M. Girvin, and R. J. Schoelkopf, Charge-insensitive qubit design derived from the Cooper pair box, Phys. Rev. A **76**, 042319 (2007).
[73] V. E. Manucharyan, J. Koch, L. I. Glazman, and M. H. Devoret, Fluxonium: Single cooper-pair, Science **326**, 113 (2009).
[74] N. Earnest, S. Chakram, Y. Lu, N. Irons, R. K. Naik, N. Leung, L. Ocola, D. A. Czaplewski, B. Baker, J. Lawrence, J. Koch, and D. I. Schuster, Realization of a Λ System with Metastable States of a Capacitively-Shunted Fluxonium, Phys. Rev. Lett. **120**, 150504 (2018).
[75] J. S. Douglas, H. Habibian, C. L. Hung, A. V. Gorshkov, H. J. Kimble, and D. E. Chang, Quantum many-body models with cold atoms coupled to photonic crystals, Nat. Photonics **9**, 326 (2015).
[76] K. Ikeda, S. Aoki, and Y. Matsuki, Hyperbolic band theory under magnetic field and dirac cones on a higher genus surface, arxiv:2104.13314.
[77] S. Guo, Y. Wang, T. Purdy, and J. Taylor, Beyond spontaneous emission: Giant atom bounded in the continuum, Phys. Rev. A **102**, 033706 (2020).
[78] F. Liu, Z. C. Yang, P. Bienias, T. Iadecola, and A. V. Gorshkov, Localization and criticality in antiblockaded 2D rydberg atom arrays, arXiv:2012.03946.
[79] P. Pudleiner and A. Mielke, Interacting bosons in two-dimensional flat band systems, Eur. Phys. J. B **88**, 207 (2015).
[80] S. Miyahara, S. Kusuta, and N. Furukawa, BCS theory on a flat band lattice, Phys. C Supercond. Appl. **460-462 II**, 1145 (2007).
[81] J. Maldacena, The large N Limit of superconformal field theories and supergravity, Adv. Theor. Math. Phys. **2**, 231 (1998).
[82] E. Witten, Anti De Sitter Space And Holography, Adv. Theor. Math. Phys. **2**, 253 (1998).